

Ordering of Spin- $\frac{1}{2}$ Excitations of the Nucleon in Lattice QCD

M.S. Mahbub^{a,b}, Waseem Kamleh^a, Derek B. Leinweber^a, Alan Ó Cais^{a,c}, Anthony G. Williams^a

^a*Special Research Centre for the Subatomic Structure of Matter, Adelaide, South Australia 5005, Australia, and Department of Physics, University of Adelaide, South Australia 5005, Australia.*

^b*Department of Physics, Rajshahi University, Rajshahi 6205, Bangladesh.*

^c*Cyprus Institute, Guy Ourisson Building, Athalassa Campus, PO Box 27456, 1645 Nicosia, Cyprus.*

Abstract

We present results for the negative parity low-lying state of the nucleon, $N_{\frac{1}{2}}^{1-}$ (1535 MeV) S_{11} , from a variational analysis method. The analysis is performed in quenched QCD with the FLIC fermion action. The principal focus of this paper is to explore the level ordering between the Roper (P_{11}) and the negative parity ground (S_{11}) states of the nucleon. Evidence of the physical level ordering is observed at light quark masses. A wide variety of smeared-smeared correlation functions are used to construct correlation matrices. A comprehensive correlation matrix analysis is performed to ensure an accurate isolation of the $N_{\frac{1}{2}}^{1-}$ state.

Key words: Baryons, Negative parity, Level crossing

PACS: 11.15.Ha, 12.38.Gc, 12.38.-t, 13.75.Gx

1. Introduction

Lattice QCD is very successful in computing many properties of hadrons from first principles. In particular, the ground state of the hadron spectrum is a well understood problem [1]. However, the excited states still prove a significant challenge. One of the long-standing puzzles in hadron spectroscopy has been the low mass of the first positive parity excitation of the nucleon, known as the Roper resonance, $N_{\frac{1}{2}}^{1+}$ (1440 MeV) P_{11} , compared to the lowest-lying negative parity partner, $N_{\frac{1}{2}}^{1-}$ (1535 MeV) S_{11} . This phenomenon cannot be observed in constituent or valence quark models where the lowest-lying odd parity state naturally occurs below the $N = \frac{1}{2}^+$ state. Similar difficulties in the level orderings also appear for the $J^P = \frac{3}{2}^+ \Delta^*(1600)$ and $\frac{1}{2}^+ \Sigma^*(1690)$ resonances.

There has been extensive research focussing on the issue of the level ordering problem using the lattice QCD approach [2–14]. One of the state-of-the-art approaches that has been used extensively in hadron spectroscopy is the ‘variational method’ [15, 16], which is based on a correlation matrix analysis. In the past the isolation of the Roper resonance was elusive with this method. However, in Refs. [17, 18] a low-lying Roper state has been identified using a correlation matrix construction with smeared-smeared correlators. Our work there mo-

tivates us to investigate the long-standing level ordering problem using the same techniques on the same lattice.

In contrast to the positive parity ground state of the nucleon, $N_{\frac{1}{2}}^{1+}$, which has a large plateau over Euclidean-time, the correlation functions for the negative parity ground state, $N_{\frac{1}{2}}^{1-}$, are short-lived giving shorter plateaus at earlier Euclidean times. Therefore, the standard analysis to extract the $N_{\frac{1}{2}}^{1-}$ ground state from small Euclidean-times may provide a mixture of ground and excited states. On the other hand, the variational method accounts for the presence of excited states in the correlation functions via correlation matrices. The masses of the energy states are then obtained by projecting the correlation matrix to eigenstates [17] providing a robust approach for extracting the energy states. In addition, considering several bases in constructing different correlation matrices provides a substantial verification of the analysis technique, in allowing the consistency of the energy states over the different basis and the reliability of the extracted eigenstates energies to be explored.

In this paper, we use the same approach as that of Ref. [17] to isolate the negative parity states of the nucleon. In particular, we focus on the negative parity state to explore the level ordering problem.

Various sweeps of gauge invariant Gaussian smearing [19] are used to construct a smeared-smeared correla-

tion function basis to form correlation matrices.

This paper is arranged as follows: Section 2 contains a brief description of the variational method. Lattice details are in Section 3. Results are discussed in Section 4 and conclusions are presented in Section 5.

2. Variational Method

The two point correlation function matrix for $\vec{p} = 0$ can be written as

$$G_{ij}^{\pm}(t) = \sum_{\vec{x}} \text{Tr}_{\text{sp}} \{ \Gamma_{\pm} \langle \Omega | \chi_i(x) \bar{\chi}_j(0) | \Omega \rangle \}, \quad (1)$$

$$= \sum_{\alpha} \lambda_i^{\alpha} \bar{\lambda}_j^{\alpha} e^{-m_{\alpha} t}, \quad (2)$$

where, Dirac indices are implicit. Here, λ_i^{α} and $\bar{\lambda}_j^{\alpha}$ are the couplings of interpolators χ_i and $\bar{\chi}_j$ at the sink and source respectively and α enumerates the energy eigenstates with mass m_{α} . $\Gamma_{\pm} = \frac{1}{2}(\gamma_0 \pm 1)$ projects the parity of the eigenstates.

Since the only t dependence comes from the exponential term, one can seek a linear superposition of interpolators, $\bar{\chi}_j u_j^{\alpha}$, such that,

$$G_{ij}(t_0 + \Delta t) u_j^{\alpha} = e^{-m_{\alpha} \Delta t} G_{ij}(t_0) u_j^{\alpha}, \quad (3)$$

for sufficiently large t_0 and $t_0 + \Delta t$. More detail can be found in Refs. [6, 20, 21]. Multiplying the above equation by $[G_{ij}(t_0)]^{-1}$ from the left leads to an eigenvalue equation,

$$[(G(t_0))^{-1} G(t_0 + \Delta t)]_{ij} u_j^{\alpha} = c^{\alpha} u_i^{\alpha}, \quad (4)$$

where $c^{\alpha} = e^{-m_{\alpha} \Delta t}$ is the eigenvalue. Similar to Eq.(4), one can also solve the left eigenvalue equation to recover the v^{α} eigenvector,

$$v_i^{\alpha} [G(t_0 + \Delta t)(G(t_0))^{-1}]_{ij} = c^{\alpha} v_j^{\alpha}. \quad (5)$$

The vectors u_j^{α} and v_i^{α} diagonalize the correlation matrix at time t_0 and $t_0 + \Delta t$ making the projected correlation matrix,

$$v_i^{\alpha} G_{ij}^{\pm}(t) u_j^{\beta} \propto \delta^{\alpha\beta}. \quad (6)$$

The parity projected, eigenstate projected correlator,

$$G_{\pm}^{\alpha} \equiv v_i^{\alpha} G_{ij}^{\pm}(t) u_j^{\alpha}, \quad (7)$$

is then analyzed using standard techniques to obtain the masses of different states.

3. Simulation Details

Our lattice ensemble is the same as that explored in Ref. [17]. It consists of 200 quenched configurations with a lattice volume of $16^3 \times 32$. Gauge field configurations are generated by using the DBW2 gauge action [22, 23] and an $O(a)$ -improved FLIC fermion action [24] is used to generate quark propagators. This action has excellent scaling properties and provides near continuum results at finite lattice spacing [25]. The lattice spacing is $a = 0.127$ fm, as determined by the static quark potential, with the scale set using the Sommer scale, $r_0 = 0.49$ fm [26]. In the irrelevant operators of the fermion action we apply four sweeps of stout-link smearing to the gauge links to reduce the coupling with the high frequency modes of the theory [27] providing $O(a)$ improvement [25]. We use the same method as in Refs. [20, 28] to determine fixed boundary effects, and the effects are significant only after time slice 25 in the present analysis. Various sweeps of gauge invariant Gaussian smearing [19] (1, 3, 7, 12, 16, 26, 35, 48 sweeps) corresponding to rms radii, in lattice units, of 0.6897, 1.0459, 1.5831, 2.0639, 2.3792, 3.0284, 3.5237, 4.1868, are applied at the source ($t = 4$) and at the sink. This is to ensure a large range of overlaps of the interpolators with the lower-lying states. The analysis is performed on eight different quark masses corresponding to pion masses of $m_{\pi} = \{0.797, 0.729, 0.641, 0.541, 0.430, 0.380, 0.327, 0.295\}$ GeV. The error analysis is performed using the jackknife method, with the χ^2/dof obtained via a covariance matrix analysis method. Our fitting method is discussed extensively in Ref. [20].

The nucleon interpolators we consider are,

$$\chi_1(x) = \epsilon^{abc} (u^{Ta}(x) C \gamma_5 d^b(x)) u^c(x), \quad (8)$$

$$\chi_2(x) = \epsilon^{abc} (u^{Ta}(x) C d^b(x)) \gamma_5 u^c(x). \quad (9)$$

We use the Dirac representation of the gamma matrices in our analysis.

4. Results

We consider several 3×3 , 4×4 , 6×6 and 8×8 correlation matrices. Each matrix is constructed with different sets of correlation functions, each set element corresponding to a different numbers of sweeps of gauge invariant Gaussian smearing at the source and sink of the $\chi_1 \bar{\chi}_1$, $\chi_2 \bar{\chi}_2$ and $\chi_1 \chi_2$ correlators [18]. This provides a large basis of operators with a variety of overlaps among energy states.

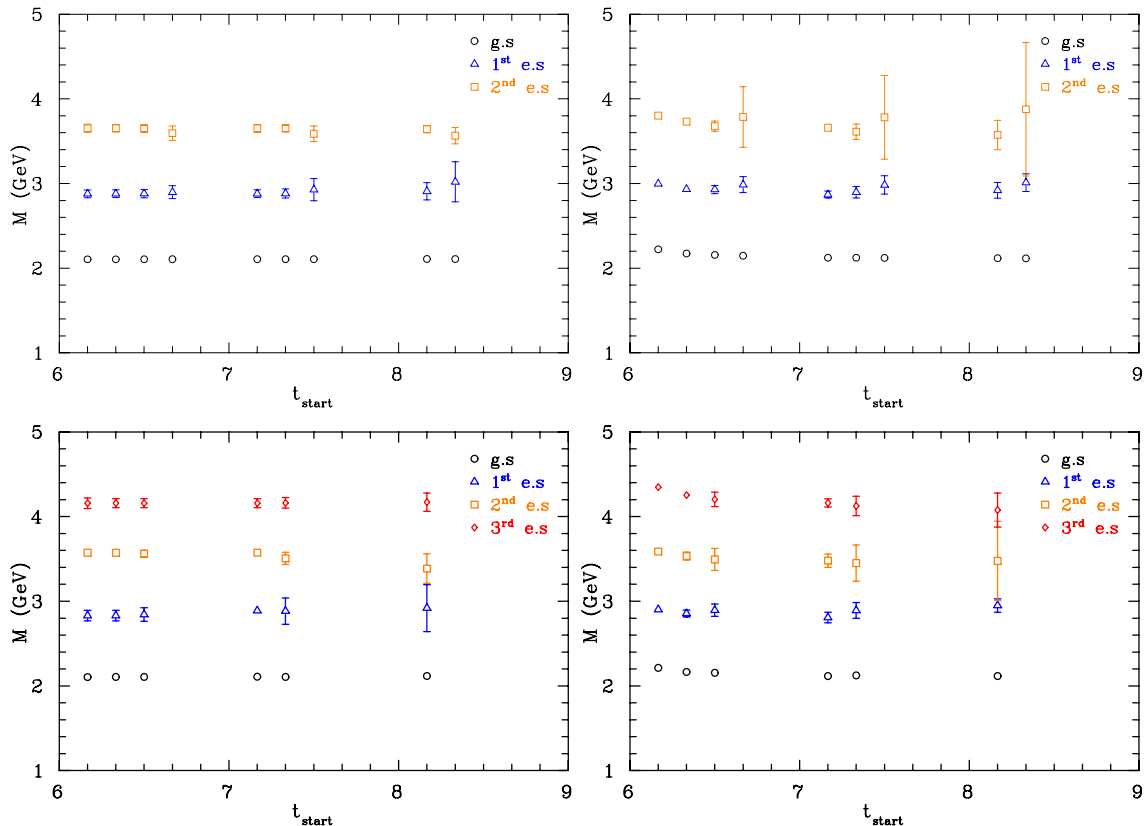


Figure 1: (colour online). Masses of the nucleon, $N_{\frac{1}{2}}^-$ states, from the projected correlation functions (left) and from the eigenvalues (right), for the 3×3 (top row) and 4×4 (bottom row) correlation matrices of $\chi_1 \bar{\chi}_1$, for the pion mass of 797 MeV. The 3×3 results correspond to the 1st combination (7,16,26 sweeps) of 3×3 matrices, while 4×4 results correspond to the 2nd combination (3,12,26,35 sweeps) of 4×4 matrices. Each set of $N_{\frac{1}{2}}^-$ ground (g.s) and excited (e.s) states masses correspond to the diagonalization of the correlation matrix for each set of variational parameters t_{start} (shown in major tick marks) and Δt (shown in minor tick marks). Here, $t_{\text{start}} \equiv t_0$ as shown in Eqs. (4) and (5).

We consider five smearing combinations (bases) $\{1=(7,16,26), 2=(7,16,35), 3=(12,16,26), 4=(12,26,35), 5=(16,26,35)\}$ for 3×3 correlation function matrices and four combinations $\{1=(1,12,26,48), 2=(3,12,26,35), 3=(3,12,26,48), 4=(12,16,26,35)\}$ for 4×4 matrices, of $\chi_1 \bar{\chi}_1$ correlation functions. In the latter case these four combinations are found optimal for the reliable extraction of the low-lying energy states shown in Ref. [17]. Including the χ_2 interpolator, which vanishes in the non-relativistic limit [29, 30], in correlation matrix analysis provides extra challenges. Nonetheless, we consider this interpolator for the reliable extraction of the negative parity ground state mass. The same bases, as discussed above for the $\chi_1 \bar{\chi}_1$ analysis, are also considered for the 3×3 and 4×4 correlation matrices of $\chi_2 \bar{\chi}_2$ correlation functions. We also consider four smearing combinations $\{1=(3,12,26), 2=(3,16,48), 3=(7,16,35), 4=(12,16,26)\}$ of 6×6 and four combina-

tions $\{1=(3,12,26,48), 2=(7,12,26,35), 3=(7,16,26,35), 4=(7,16,35,48)\}$ for 8×8 matrices of $\chi_1 \chi_2$ correlation functions.

In Fig. 1, masses from the projected correlation functions and from the eigenvalues are shown for the 3×3 and 4×4 correlation matrices. We refer to the lowest lying state as the ground state in the negative parity sector. As in Refs. [17, 20], masses from the projected correlation functions for the low-lying states are very consistent over the variational parameters of t_{start} and Δt , in particular, the negative parity ground state is robust. However, a deteriorating signal to noise is evident for larger t_{start} and Δt values, particularly for the excited states. In contrast, the mass from the eigenvalue analysis shows significant dependence on the variational parameters. Therefore, exposing a mass from the projected correlation functions is again proved to be more reliable than from the eigenvalues [17].

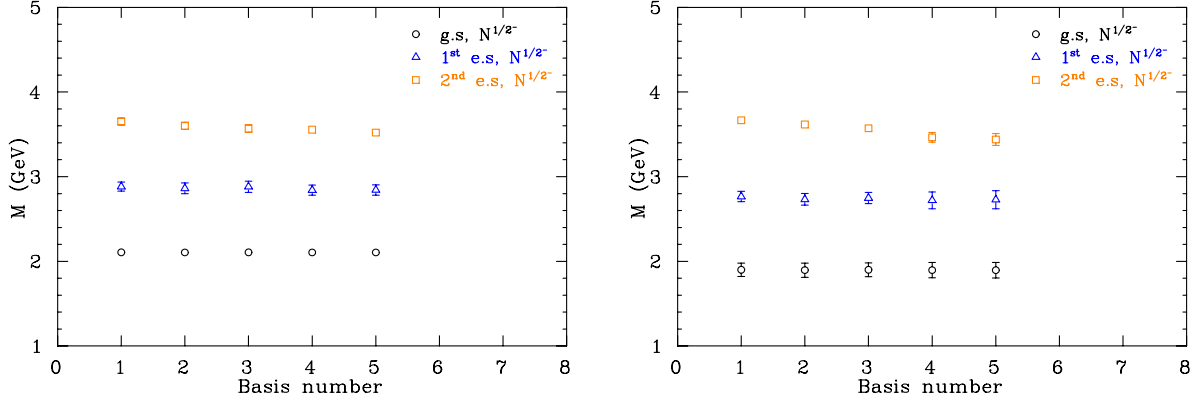


Figure 2: (color online). Masses of the nucleon, $N_{1/2}^{1-}$ - states, from projected correlation functions as shown in Eq. (7) for the pion mass of 797 MeV (left) and 380 MeV (right). Numbers in the horizontal scale correspond to each combination of smeared 3×3 correlation matrices of $\chi_1 \bar{\chi}_1$. For instance, 1 and 2 correspond to the combinations of (7,16,26) and (7,16,35) sweeps, respectively and so on, as discussed in the text following Eq. (9).

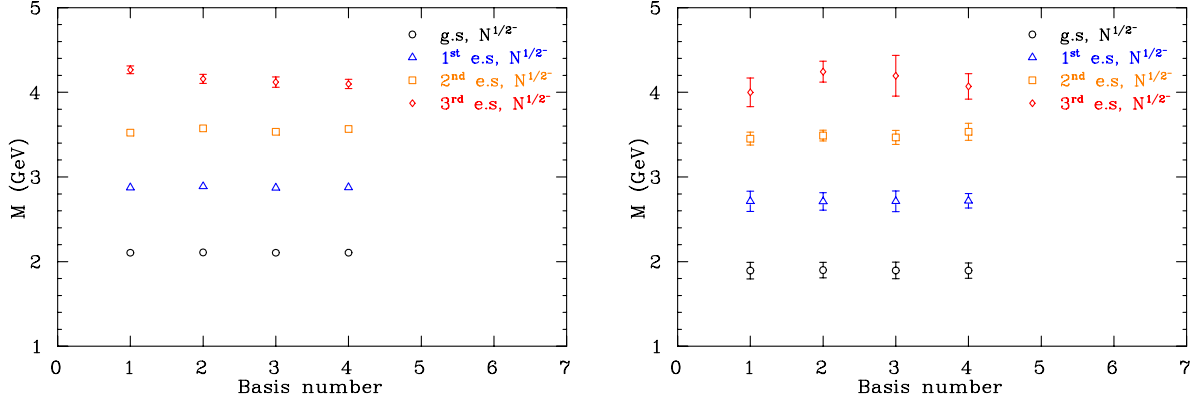


Figure 3: (color online). As in Fig. 2, but for the 4×4 correlation matrices of $\chi_1 \bar{\chi}_1$.

From a series of t_{start} and Δt , a single mass is selected for one set of t_{start} and Δt by the selection criteria discussed in Ref. [20], where we prefer larger value of $t_{\text{start}} + \Delta t$ [21]. In cases where a larger $t_{\text{start}} + \Delta t$ provides a poor signal-to-noise ratio, for example $(t_{\text{start}}, \Delta t) = (7, 3)$ (top left graph of Fig. 1), we prefer a little lower $t_{\text{start}} + \Delta t$ value, for example $(t_{\text{start}}, \Delta t) = (7, 2)$, and we follow this procedure for each quark mass, as discussed in Ref. [18].

In Fig. 2, masses extracted from all the combinations of 3×3 matrices (from 1st to 5th) are shown for the pion mass of 797 and 380 MeV. Here the negative parity ground and the first excited states are very consistent for all the 3×3 bases. The second excited state shows some smearing dependence [20] which is also observed in Ref. [17] as this highest excited state must accommo-

date all remaining spectral strength.

In Fig. 3, masses extracted from all the combinations of 4×4 matrices of $\chi_1 \bar{\chi}_1$ are shown. In Ref. [17], the three low-lying states were consistent over these four bases for the positive parity excited states and similarly consistent results are also observed in this negative parity correlation matrix analysis, again illustrating the robustness of the method [17]. A smearing dependency for the highest excited state is also noticed in this 4×4 analysis, which is to be expected.

It is noted that although the 3×3 correlation matrix analyses are successful for all the eight quark masses, the 4×4 correlation matrix analyses are successful only for the six heavier quarks. In this case, the signal-to-noise ratio for the lighter quarks deteriorates more rapidly than the heavier quarks. As a result the vari-

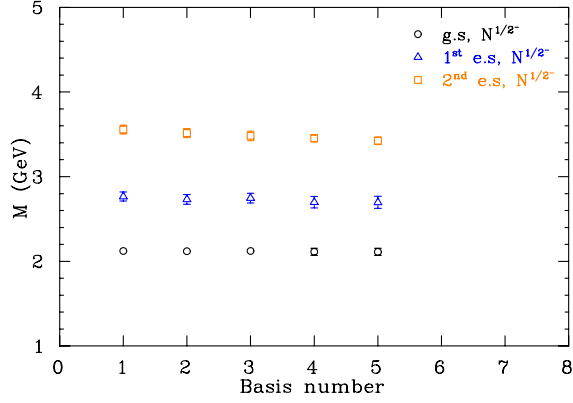


Figure 4: (color online). Masses of the nucleon, $N_{\frac{1}{2}}^{1-}$ - states, from projected correlation functions as shown in Eq. (7) for the pion mass of 797 MeV. Numbers in the horizontal scale correspond to each combination of smeared 3×3 correlation matrices of $\chi_2\bar{\chi}_2$. For instance, 1 and 2 correspond to the combinations of (7,16,26) and (7,16,35) sweeps, respectively and so on.

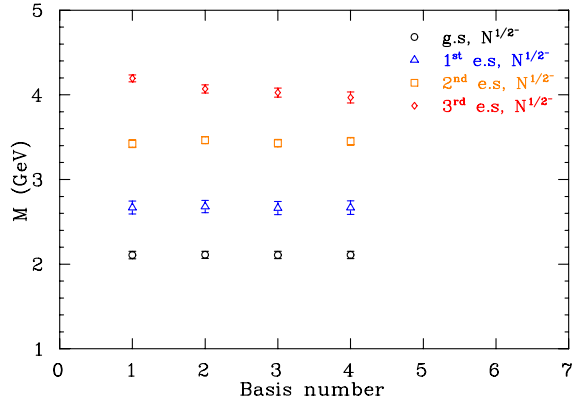


Figure 5: (color online). Masses of the nucleon, $N_{\frac{1}{2}}^{1-}$ - states, from projected correlation functions as shown in Eq. (7) for the pion mass of 797 MeV. Numbers in the horizontal scale correspond to each combination of smeared 4×4 correlation matrices of $\chi_2\bar{\chi}_2$. For instance, 1 and 2 correspond to the combinations of (1,12,26,48) and (3,12,26,35) sweeps, respectively and so on.

ational analysis for 4×4 correlation matrices for the lighter two quarks is unsuccessful.

We now discuss the 3×3 and 4×4 correlation matrices of $\chi_2\bar{\chi}_2$. As the χ_2 interpolator is very challenging to perform a simulation with and the signal-to-noise ratio of the $\chi_2\bar{\chi}_2$ correlator deteriorates rapidly, the diagonalization of 3×3 (Fig. 4) and 4×4 (Fig. 5) matrices are only successful for the four heavier quark masses. The energy states revealed by the χ_2 spin-flavour analysis are also very consistent as with the $\chi_1\bar{\chi}_1$ analysis. In particular, the $N_{\frac{1}{2}}^{1-}$ ground state is again robust.

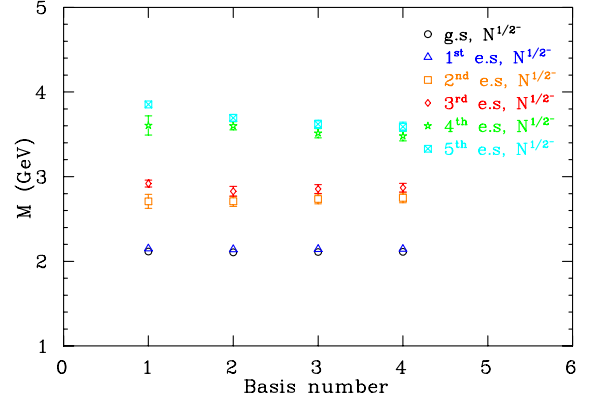


Figure 6: (color online). Masses of the nucleon, $N_{\frac{1}{2}}^{1-}$ - states, from projected correlation functions as shown in Eq. (7) for the pion mass of 797 MeV. Numbers in the horizontal scale correspond to each combination of smeared 6×6 correlation matrices of $\chi_1\chi_2$. For instance, 1 and 2 correspond to the combinations of (3,12,26) and (3,16,48) sweeps, respectively and so on.

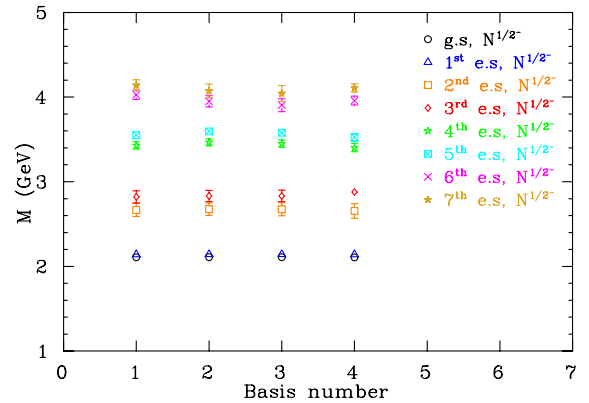


Figure 7: (color online). As in Fig. 6, but for the 8×8 correlation matrices of $\chi_1\chi_2$.

We now consider the 6×6 and 8×8 analyses involving both χ_1 and χ_2 , where linear combinations of χ_1 and χ_2 are utilized to isolate eigenstates.

The lowest two energy states extracted with the 6×6 basis are nearly degenerate as illustrated in Fig. 6. An explanation for these two nearby degenerate states is provided by the quark model. In the quark model based on SU(6) symmetry, four decuplet and two octet states contribute to provide the 56 representation of SU(6). The nucleon and Roper belongs to the ground and excited 56 representation of SU(6) symmetry respectively. On the other hand, the odd parity ground (1535 MeV) and (1650 MeV) states belong to the negative parity, $L = 1$, 70 plet of SU(6). As three spin- $\frac{1}{2}$ quarks may

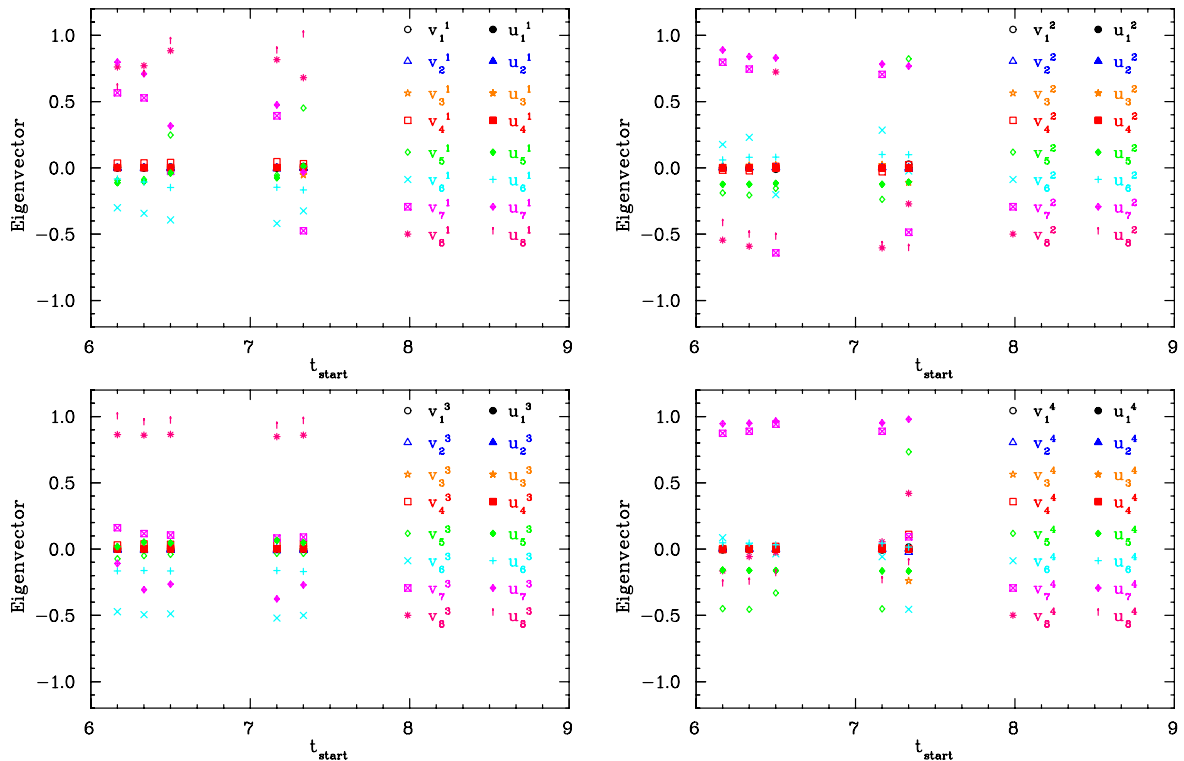


Figure 8: (color online). Eigenvector values, v_i^α and u_i^α , as shown in Eq. (7), for the first (lowest) state (top left), second (top right), third (bottom left) and fourth (bottom right) energy states. The figure corresponds to the pion mass of 797 MeV and for the 2nd combination (7,12,26,35 sweeps) of 8×8 correlation matrix of $\chi_1\chi_2$. In the legend, superscripts stand for the energy state and subscripts represent eigenvector contributions of interpolators to make a state of interest, e.g. $v_1^1, v_3^1, v_5^1, v_7^1$ and $v_2^1, v_4^1, v_6^1, v_8^1$ correspond to the contributions from χ_1 and χ_2 operator for the ground state respectively, with larger subscript values corresponding to larger smearings. To be specific, component v_1^α and v_2^α correspond to the low smearing sweep count of 7, v_3^α and v_4^α for the sweep count of 12, and so on. Errors are suppressed for clarity.

give rise to a total spin of $s = \frac{1}{2}$ or $\frac{3}{2}$, the $L = 1$ state can couple two different ways to provide a $J = \frac{1}{2}$ state, i.e. $\vec{1} + \vec{1} = \frac{1}{2}$ or $\vec{1} + \vec{3} = \frac{1}{2}$, hence providing two orthogonal spin- $\frac{1}{2}$ states in the $L = 1$, 70 plet representation. Both of these negative-parity states have a width of ≈ 150 MeV. It is interesting that the $\chi_1\chi_2$ spin flavour combinations successfully isolate the nearly degenerate ground states, in accord with the SU(6) quark model. This approximate degeneracy is repeated throughout our observed spectrum.

In Fig. 7, similar nearly degenerate low-lying states from the 8×8 analysis are evident as in the 6×6 case. We note that, only the analysis involving χ_2 is able to extract a new second excited state. This state is close to the experimentally identified one star, $N_{\frac{1}{2}}^-$ (2090 MeV) S_{11} state which has ≈ 400 MeV of width. Further analysis is required with higher statistics to explore the propagation of these states to light quark masses.

The eigenvectors (Fig. 8) indicate that both χ_1 and

χ_2 operators have nontrivial contributions in extracting the two lowest lying states. In particular, the contributions to the ground state is significantly dominated by the χ_2 interpolator, whereas a larger dominance of the χ_1 interpolator is evident for the first excited state, revealing a diminished role for the scalar diquark in the negative parity sector. This observation is in accord with Ref. [14].

It has already been mentioned that only the correlation matrix analysis involving χ_2 spin-flavour combinations is able to extract the third energy state. It is evident from the eigenvector contributions that this energy state is almost a pure χ_2 state (bottom left graph). The fourth energy state is dominated by the χ_1 operator. It is evident that larger smearing, i.e. sweep count of 35, dominates over low smearing levels in isolating these eigen-energy states.

The extracted masses from all the bases are very consistent. In particular, the ground state is robust. There-

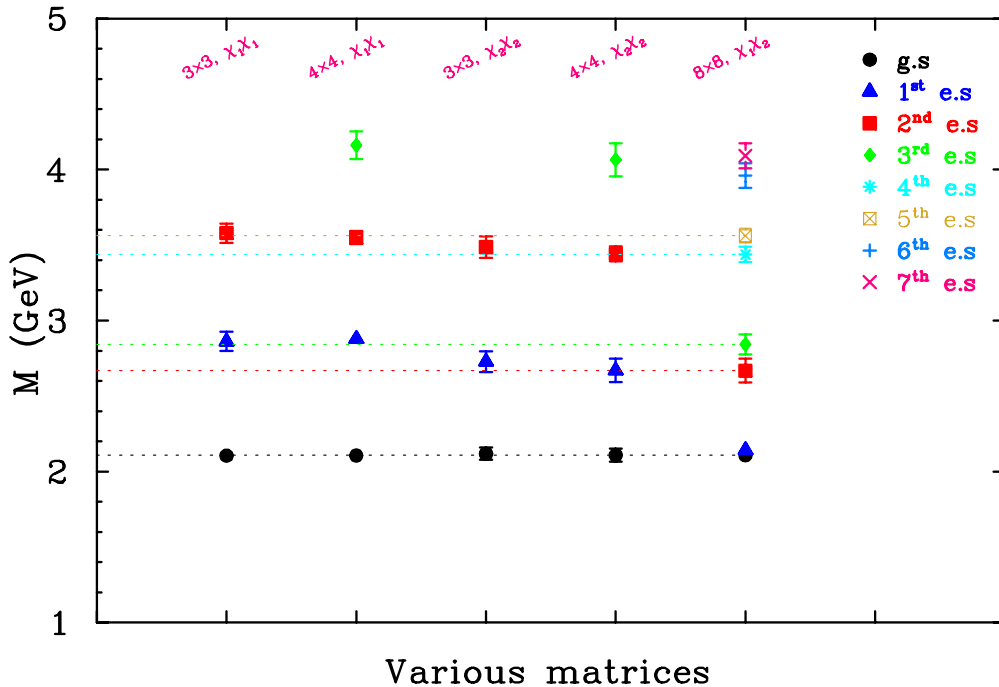


Figure 9: (color online). Masses of the nucleon, $N_{\frac{1}{2}}^{-}$ states, for all the various dimensions of correlation matrices as labelled on the upper horizontal axis. Dotted lines are drawn to aid in illustrating the consistency of the results. Figure corresponds to the pion mass of 797 MeV.

fore, all the bases are considered in performing the following systematic error analysis.

A systematic error analysis as that of Ref. [17] is performed to calculate the systematic errors associated with the choice of basis, with $\sigma_b = \sqrt{\frac{1}{N_b-1} \sum_{i=1}^{N_b} (M_i - \bar{M})^2}$, where N_b is the number of bases. This analysis is performed over all the bases considered. The masses are averaged over the bases and errors (average statistical errors and systematic errors associated with basis choices) are combined in quadrature, $\sigma = \sqrt{\sigma_s^2 + \sigma_b^2}$.

At this stage, we examine the consistency of the low-lying energy states over different dimensions of the correlation matrices in Fig. 9. Whereas a non-trivial mixing of χ_1 and χ_2 is required to isolate the two lowest lying states, the near trivial mixing in the third and fourth (χ_2 dominated, χ_1 dominated) and similarly in the fifth and sixth states of the 8×8 analysis is manifest.

In Fig. 10, the negative parity ground state results are presented for all the correlation matrices (masses are given in Table 1). The positive parity ground state (nucleon) and Roper state results are taken from Ref. [17] for comparison. Regarding the level ordering problem, we do not see the physical level ordering for the three

heavier quark masses, where the $N_{\frac{1}{2}}^{-}$ state lies below the Roper, $N_{\frac{1}{2}}^{+}$, state. A coincidence of the Roper and $N_{\frac{1}{2}}^{-}$ states occurs at pion mass of 380 MeV and the physical level ordering is observed at pion masses below 380 MeV.

For evidence of the physical level ordering, we calculate the correlated jackknife error over the ratio of masses of Roper to the negative parity state. For our second lightest quark mass the result is $0.947^{+0.047}_{-0.047}$ and for the lightest quark mass it is $0.909^{+0.054}_{-0.059}$, providing strong evidence of a physical level ordering. Little evidence is found that our extracted lattice $N_{\frac{1}{2}}^{-}$ state approaches the physical state. We note that chiral physics is significantly altered in quenched QCD for $m_\pi < 250$ MeV. Moreover, the finite volume of the lattice will also become significant in this regime. Future calculations of negative parity states from the variational approach addressing the light quark masses should be done on large volume lattices in $2 + 1$ flavour QCD.

At our heavier three quark masses the $N_{\frac{1}{2}}^{-}$ state lies below the S-wave $N + \pi$ state indicative of attractive interactions. The lower values of the $N + \pi$ scattering state at light pion masses implies that the couplings of our interpolators are small for the two particle $N + \pi$ state at these pion masses.

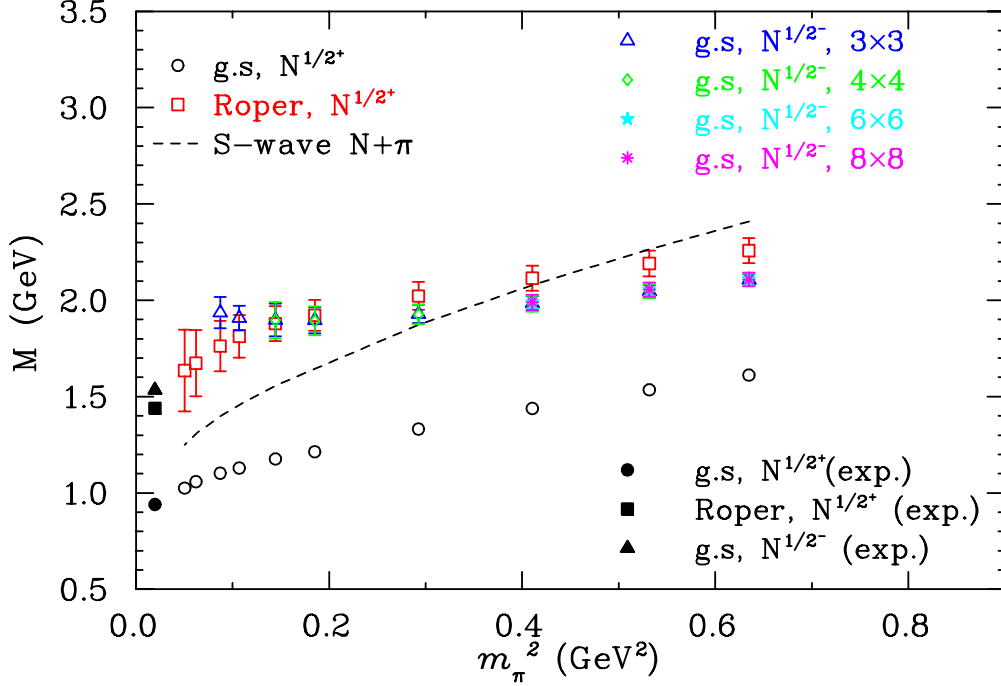


Figure 10: (color online). Mass of the nucleon, $N_{\frac{1}{2}^+}$, Roper $N_{\frac{1}{2}^+}$ (P_{11}) and the negative parity ground state, $N_{\frac{1}{2}^-}$ (S_{11}) are presented. The combination of errors in quadrature is shown. The ground and Roper states are taken from Ref. [17] for comparison with the negative parity ground state. The black filled symbols are the experimental values.

Table 1: Mass of the negative parity ground state of the nucleon, $N_{\frac{1}{2}^-}$, for 3×3 , 4×4 , 6×6 and 8×8 correlation matrices. Masses are averaged over the bases described in the text and errors are a combination of average statistical errors over the bases and systematic errors for choice of basis.

aM_π	$aM_{\text{g.s.}}^{N_{\frac{1}{2}^-}} (3 \times 3)$	$aM_{\text{g.s.}}^{N_{\frac{1}{2}^-}} (4 \times 4)$	$aM_{\text{g.s.}}^{N_{\frac{1}{2}^-}} (6 \times 6)$	$aM_{\text{g.s.}}^{N_{\frac{1}{2}^-}} (8 \times 8)$
0.5141(19)	1.358(19)	1.358(20)	1.362(21)	1.359(23)
0.4705(20)	1.320(21)	1.320(22)	1.327(22)	1.326(24)
0.4134(22)	1.279(25)	1.278(26)	1.285(22)	1.283(25)
0.3490(24)	1.244(30)	1.243(33)	-	-
0.2776(24)	1.223(44)	1.221(48)	-	-
0.2452(24)	1.224(55)	1.223(61)	-	-
0.2110(27)	1.231(40)	-	-	-
0.1905(31)	1.249(53)	-	-	-

5. Conclusions

An extensive analysis has been performed to address the issue of the level ordering problem in the nucleon sector through the variational approach. A similar method to that of Ref. [17] is used to explore this long-standing problem. The physical level ordering between the Roper and $N_{\frac{1}{2}^-}$ ground states in a pion mass region of 295 – 380 MeV is observed. However, an identifica-

tion of a low-lying negative-parity state in the Physical quark mass regime remains.

Acknowledgments

This research was undertaken on the NCI National Facility in Canberra, Australia, which is supported by the Australian Commonwealth Government. We also acknowledge eResearch SA for generous grants of su-

percomputing time which have enabled this project. This research is supported by the Australian Research Council.

References

- [1] S. Durr, et al., *Science* 322 (2008) 1224–1227. [arXiv:0906.3599](#),
- [2] S. Sasaki, T. Blum, S. Ohta, *Phys. Rev. D* 65 (2002) 074503. [arXiv:hep-lat/0102010](#).
- [3] D. G. Richards, et al., *Nucl. Phys. Proc. Suppl.* 109A (2002) 89–95. [arXiv:hep-lat/0112031](#).
- [4] F. X. Lee, et al., *Nucl. Phys. Proc. Suppl.* 119 (2003) 296–298. [arXiv:hep-lat/0208070](#).
- [5] S. Sasaki, *Prog. Theor. Phys. Suppl.* 151 (2003) 143–148. [arXiv:nucl-th/0305014](#).
- [6] W. Melnitchouk, et al., *Phys. Rev. D* 67 (2003) 114506. [arXiv:hep-lat/0202022](#).
- [7] D. Brommel, et al., *Phys. Rev. D* 69 (2004) 094513. [arXiv:hep-ph/0307073](#).
- [8] N. Mathur, et al., *Phys. Lett. B* 605 (2005) 137–143. [arXiv:hep-ph/0306199](#).
- [9] K. Sasaki, S. Sasaki, T. Hatsuda, *Phys. Lett. B* 623 (2005) 208–217. [arXiv:hep-lat/0504020](#).
- [10] D. Guadagnoli, M. Papinutto, S. Simula, *Phys. Lett. B* 604 (2004) 74–81. [arXiv:hep-lat/0409011](#).
- [11] S. Basak, et al., *Phys. Rev. D* 76 (2007) 074504. [arXiv:\protect\vrulewidth0pt\protect\href{http://arxiv.org/abs/0709.0008}\{arXiv:0709.0008\}](#) [[hep-lat](#)].
- [12] J. M. Bulava, et al., *Phys. Rev. D* 79 (2009) 034505. [arXiv:0901.0027](#),
- [13] J. Bulava, et al. [arXiv:1004.5072](#).
- [14] G. P. Engel, C. B. Lang, M. Limmer, D. Mohler, A. Schafer [arXiv:1005.1748](#).
- [15] C. Michael, *Nucl. Phys.* B259 (1985) 58.
- [16] M. Luscher, U. Wolff, *Nucl. Phys.* B339 (1990) 222–252.
- [17] M. S. Mahbub, et al., *Phys. Lett. B* 679 (2009) 418–422. [arXiv:0906.5433](#),
- [18] M. S. Mahbub, A. O. Cais, W. Kamleh, D. B. Leinweber, A. G. Williams [arXiv:1004.5455](#).
- [19] S. Gusken, *Nucl. Phys. Proc. Suppl.* 17 (1990) 361–364.
- [20] M. S. Mahbub, et al., *Phys. Rev. D* 80 (2009) 054507. [arXiv:0905.3616](#),
- [21] B. Blossier, M. Della Morte, G. von Hippel, T. Mendes, R. Sommer, *JHEP* 04 (2009) 094. [arXiv:0902.1265](#),
- [22] T. Takaishi, *Phys. Rev. D* 54 (1996) 1050–1053.
- [23] P. de Forcrand, et al., *Nucl. Phys.* B577 (2000) 263–278. [arXiv:hep-lat/9911033](#)
- [24] J. M. Zanotti, et al., *Phys. Rev. D* 65 (2002) 074507. [arXiv:hep-lat/0110216](#).
- [25] J. M. Zanotti, B. Lasscock, D. B. Leinweber, A. G. Williams, *Phys. Rev. D* 71 (2005) 034510. [arXiv:hep-lat/0405015](#).
- [26] R. Sommer, *Nucl. Phys.* B411 (1994) 839–854. [arXiv:hep-lat/9310022](#)
- [27] C. Morningstar, M. J. Peardon, *Phys. Rev. D* 69 (2004) 054501. [arXiv:hep-lat/0311018](#)
- [28] B. G. Lasscock, et al., *Phys. Rev. D* 72 (2005) 074507. [arXiv:hep-lat/0504015](#).
- [29] D. B. Leinweber, R. M. Woloshyn, T. Draper, *Phys. Rev. D* 43 (1991) 1659–1678.
- [30] D. B. Leinweber, *Phys. Rev. D* 51 (1995) 6383–6393. [arXiv:nucl-th/9406001](#).